RESEARCH ARTICLE

WILEY

Superaccurate effective elastic moduli via postprocessing in computational homogenization

Matti Schneider

Karlsruhe Institute of Technology (KIT),
Institute of Engineering Mechanics,
Karlsruhe, Germany

Correspondence
Matti Schneider, Karlsruhe Institute of
Technology (KIT), Institute of Engineering
Mechanics, Karlsruhe, Germany.
Email: matti.schneider@kit.edu

Abstract

With the complexity of modern microstructured materials, computational homogenization methods have been shown to provide accurate estimates of their effective mechanical properties, reducing the involved experimental effort considerably. After solving the balance of linear momentum on the microscale, the effective stress is traditionally computed through volume averaging the microscopic stress field. In the work at hand, we exploit the idea that averaging the elastic energy may lead to much more accurate effective elastic properties than through stress averaging. We show that the accuracy is roughly doubled when using energy equivalence instead of strain equivalence for compatible iterates of iterative schemes. Thus, to achieve a prescribed accuracy, the necessary effort is roughly reduced by a factor of two. In addition to the theory, we provide a handbook for utilizing these ideas for modern solvers prominent in FFT-based micromechanics. We demonstrate the superiority of energy averaging through computational examples, discuss the peculiarities of polarization methods with their non-compatible iterates and expose a superaccuracy phenomenon occurring for the linear conjugate gradient method.

KEYWORDS
computational homogenization, effective stiffness, energy equivalence, FFT-based methods, Hill–Mandel condition

1 | INTRODUCTION

1.1 | State of the art

In the last decades, computational homogenization methods have reached a degree of sophistication which permits their use as general-purpose tools for materials with rather complex microstructures, see the detailed review article.[1] Once the constitutive behavior of the individual phases constituting the microstructured material is fixed, the computational engineer has to face (at least) three sources of error. For a start, a large class of microstructured materials come with a random microstructure, necessitating the use of stochastic homogenization approaches.[2,3] The effective properties of the material only emerge by considering sufficiently large cells, the so-called representative volume elements (RVEs).[4-6] When working with computational cells of finite size, the discrepancy between the effective properties of the medium and the

---

apparent properties of the cell under consideration needs to be quantified and made as small as desired. It is well-known that this error involves a random part, accounting for the fluctuations of the apparent properties on cells of finite size, and a systematic part, which is caused by additional correlations introduced by working on cells of finite size, see Gloria and Otto.[7] Moreover, the artificially introduced boundary conditions play a decisive role,[8-10] with periodic boundary conditions typically providing more accurate results, at least provided a suitable periodization of the material is used.[11-13] The second source of error emerges once a computational cell is fixed. To solve the corrector problem on a computer, the equations need to be discretized. Classical approaches may be used for this purpose, including finite difference,[14] finite element,[15] and finite volume[16] approaches. However, multiphase materials with complex microstructures come with their specific challenges, for example, featuring several thousands of inclusions with intricate shapes. In particular, generating interface-conforming meshes turns out to be challenging in three spatial dimensions.[17] Moreover, with the advent of modern digital image techniques,[18,19] it became natural to work with an implicit microstructure description on voxel meshes. In particular, the exact location of the interfaces between the phases is not accessible for such a description. A positive side effect of such homogenization problems is that the microstructure is typically given on a rectangular box, simplifying the (outer) boundary description, at least. With these facts in mind, a set of dedicated discretization methods has been developed, including voxel-based finite element methods[20-22] and spectral techniques.[23,24] The second error on our list comprises the error introduced by the discretization used, in particular related to the width of the underlying mesh.

Last but not least, once a discretization is chosen, the emerging discretized equations need to be solved, giving rise to the third error. Indeed, such numerical techniques come with a convergence rate, which in turn is responsible for the number of iterations required to solve the equations to the desired accuracy. For discretizations on a regular grid, a number of dedicated computational techniques has been developed, including methods based on the fast Fourier transform (FFT). These methods utilize the regular structure of a Cartesian grid to construct proper preconditioners for classical conjugate gradient (CG)[25-27] or Newton-CG methods.[28,29] Also, closely related solvers were introduced, see the recent review articles[30-33] within the framework of the Lippmann–Schwinger equation.[34-36] A key characteristic of the solvers is that the condition numbers of the preconditioned equations is independent of the mesh size, only depending on the material contrast, sometimes even bounded independently of it.[37]

When facing a problem in computational homogenization, the working engineer has to deal with all three error sources, which in turn are responsible for the runtime. For instance, if the considered cell increases its volume by a factor of eight, the runtime will typically increase at least by a factor of eight, as well. On the other end of the spectrum, doubling the desired accuracy of the computational solution method also doubles the runtime, in general, when linearly converging solvers—more or less unavoidable for large-scale problems—are used.

1.2 | Contributions

The work at hand is focused on the third error exploiting a clever postprocessing of the local solution fields. To be more precise, there is a "folklore theorem" in computational homogenization which states that the effective elastic properties converge faster than the local solution fields. This paradigm concerns the accuracy of discretizations, and is based on the fact that averaging profits from cancellations which adversely affect the convergence of the local fields. A mathematically precise statement can be found in Ye and Chung.[38(Thm. 5)]

The starting point of the article at hand was the question whether this principle, which concerned difference between the discretized and the continuous solution, could also be exploited for a *fixed discretization* and various solution methods. To be more precise and for linear elastic constituents, traditionally the workflow proceeds by first computing an approximate solution of the corrector equation, followed by averaging the associated local stress field to obtain an estimate for the corresponding column in the (matrix representation of) effective stiffness. In the work at hand, we show that it is actually more accurate to compute all six (in three spatial dimensions) independent local strain fields first, store them on hard disk, and to compute the individual entries of the effective stiffness through energy averaging. We demonstrate—both theoretically and through computational examples—that this simple postprocessing approach roughly doubles the accuracy of the computed effective[*] stiffness relative to the exact effective stiffness associated to this discretization. In turn, if a specific degree of accuracy is desired, it is actually sufficient to solve the discretized corrector equation only to roughly half accuracy. In particular, about half of the runtime may be saved with such an approach.[39]

After this article has been accepted, the author has learnt that the material presented in section 2 has been discussed in a different context by Bellis et al.,[39] section 4.2.

This work is organized as follows. A theoretical development is given in Section 2, introducing the notation and giving the main argument. Subsequently, Section 3 discusses how to exploit these theoretical findings in practice, working out the specifics for FFT-based solution methods. In particular, it is shown how to deal with iterative schemes that produce non-compatible iterates. Also, it is shown that the linear conjugate gradient method comes with an interesting feature, that is, the spatially averaged stress converges faster in one fixed direction than in the other directions, see Appendix A.

The developments are restricted to linear elasticity, which forms the point of departure for homogenizing nonlinear properties and has recently been utilized also to estimate nonlinear properties of composites.[40,41] Possible extensions are discussed in the conclusion section.

2 | THE FUNDAMENTAL ESTIMATE

Following standard material in computational homogenization,[42] let us consider a rectangular computational cell

$$Q = [0, L_1] \times [0, L_2] \times \cdots \times [0, L_d], \tag{1}$$

in d dimensions, and suppose a microscopic stiffness distribution

$$\mathbb{C} : Q \to L(\mathrm{Sym}(d)), \tag{2}$$

is given, which associates a stiffness tensor $\mathbb{C}(x)$ to every microscopic point $x \in Q$. We assume the stiffness tensors $\mathbb{C}(x)$ to satisfy the minor and major symmetries, that is, we consider them as symmetric linear operators on $\mathrm{Sym}(d)$, the symmetric $d \times d$-tensors. Moreover, to make the derivations well-defined, we assume that the stiffness tensors (2) are essentially bounded by a constant $L > 0$ and pointwise positive semi-definite. For any prescribed strain $\bar{\varepsilon} \in \mathrm{Sym}(d)$, the (periodic) corrector displacement field $u_{\bar{\varepsilon}} \in H^1_\#(Q; \mathbb{R}^d)$, solves the equation

$$\mathrm{div}\, \mathbb{C} : (\bar{\varepsilon} + \nabla^s u_{\bar{\varepsilon}}) = 0, \tag{3}$$

where ∇^s refers to the symmetrized gradient and $:$ is the double contraction. The effective stress

$$\bar{\sigma}_{\bar{\varepsilon}} = \left\langle \mathbb{C} : (\bar{\varepsilon} + \nabla^s u_{\bar{\varepsilon}}) \right\rangle_Q, \tag{4}$$

is computed by volume averaging, which is defined by

$$\langle q \rangle_Q \equiv \frac{1}{|Q|} \int_Q q(x)\, dx, \tag{5}$$

for any vectorial or tensorial quantity q. As the constitutive law is linear, this process gives rise to an effective stiffness tensor $\mathbb{C}^{\mathrm{eff}} \in L(\mathrm{Sym}(d))$, implicitly defined by

$$\mathbb{C}^{\mathrm{eff}} : \bar{\varepsilon} = \bar{\sigma}_{\bar{\varepsilon}}, \tag{6}$$

for any $\bar{\varepsilon} \in \mathrm{Sym}(d)$. The effective stiffness tensor $\mathbb{C}^{\mathrm{eff}}$ inherits the symmetry property (i.e., the major symmetries) from the microscopic stiffness distribution (2). This may be seen, for instance, from the alternative representation

$$\bar{\xi} : \mathbb{C}^{\mathrm{eff}} : \bar{\varepsilon} = \left\langle (\bar{\xi} + \nabla^s u_{\bar{\xi}}) : \mathbb{C} : (\bar{\varepsilon} + \nabla^s u_{\bar{\varepsilon}}) \right\rangle_Q, \quad \bar{\xi}, \bar{\varepsilon} \in \mathrm{Sym}(d), \tag{7}$$

which is a direct consequence of integration by parts.

The purpose of this work is to exploit the differences between strain equivalence (6) and energy equivalence (7) for approximate solutions to the corrector equation (3). For any fixed $\bar{\varepsilon} \in \mathrm{Sym}(d)$, let us write

$$\varepsilon^* = \bar{\varepsilon} + \nabla^s u_{\bar{\varepsilon}}. \tag{8}$$

For any field $\varepsilon \in L^2(Q; \mathrm{Sym}(d))$, we may estimate

$$\left\| \langle \mathbb{C} : \varepsilon \rangle_Q - \langle \mathbb{C} : \varepsilon^* \rangle_Q \right\| \leq \| \mathbb{C} : (\varepsilon - \varepsilon^*) \|_{L^2} \leq L \ \| \varepsilon - \varepsilon^* \|_{L^2}, \tag{9}$$

in terms of the L^2-norm

$$\| \varepsilon \|_{L^2} = \sqrt{\langle \| \varepsilon \|^2 \rangle_Q} \equiv \sqrt{\langle \varepsilon : \varepsilon \rangle_Q}, \tag{10}$$

and an upper bound L on the eigenvalues of the local stiffnesses $\mathbb{C}(x)$. The estimate (9) reveals that, up to a constant, the accuracy of the effective stress coincides with the accuracy of the local strain field, measured in the L^2-norm.

Fortunately, we can construct a better approximation to the effective stiffness as follows. For this purpose, let $\overline{\xi} \in \mathrm{Sym}(d)$ be arbitrary, and write

$$\xi^* = \overline{\xi} + \nabla^s u_{\overline{\xi}}. \tag{11}$$

For arbitrary $w, v \in H^1_{\#}(Q; \mathbb{R}^d)$ write

$$\varepsilon = \overline{\varepsilon} + \nabla^s w \quad \text{and} \quad \xi = \overline{\xi} + \nabla^s v. \tag{12}$$

Then, the following identity holds

$$\langle (\varepsilon - \varepsilon^*) : \mathbb{C} : (\xi - \xi^*) \rangle_Q = \langle \varepsilon : \mathbb{C} : \xi \rangle_Q - \overline{\xi} : \mathbb{C}^{\mathrm{eff}} : \overline{\varepsilon}. \tag{13}$$

Before coming to the derivation, let us briefly discuss the ramifications. By the Cauchy–Schwarz inequality, and invoking the upper bound L to the application of the stiffness, we observe

$$\left| \langle \varepsilon : \mathbb{C} : \xi \rangle_Q - \overline{\xi} : \mathbb{C}^{\mathrm{eff}} : \overline{\varepsilon} \right| = \langle (\varepsilon - \varepsilon^*) : \mathbb{C} : (\xi - \xi^*) \rangle_Q$$

$$\leq \| \varepsilon - \varepsilon^* \|_{L^2} \| \mathbb{C} : (\xi - \xi^*) \|_{L^2}$$

$$\leq L \ \| \varepsilon - \varepsilon^* \|_{L^2} \| \xi - \xi^* \|_{L^2}. \tag{14}$$

In particular, if we choose $\overline{\xi} = \overline{\varepsilon}$ and $\xi = \varepsilon$, we obtain the bound

$$\left| \langle \varepsilon : \mathbb{C} : \varepsilon \rangle_Q - \overline{\varepsilon} : \mathbb{C}^{\mathrm{eff}} : \overline{\varepsilon} \right| \leq L \ \| \varepsilon - \varepsilon^* \|^2_{L^2}. \tag{15}$$

Compared to strain averaging (9), energy averaging involves the square of the L^2-error of the local strain fields. In particular, for computational methods which seek close approximations to the true fields, computing the effective stiffness via energy equivalence, see Section 3 below, leads to essentially double precision than achievable with strain equivalence.

Let us discuss how to show that the identity (13) holds. Let us split the left-hand side of Equation (13)

$$\langle (\varepsilon - \varepsilon^*) : \mathbb{C} : (\xi - \xi^*) \rangle_Q = \langle (\varepsilon - \varepsilon^*) : \mathbb{C} : \xi \rangle_Q - \langle (\varepsilon - \varepsilon^*) : \mathbb{C} : \xi^* \rangle_Q. \tag{16}$$

Writing the second summand in the form

$$\langle (\varepsilon - \varepsilon^*) : \mathbb{C} : \xi^* \rangle_Q = \langle (\nabla^s (w - u_{\overline{\varepsilon}})) : \mathbb{C} : \xi^* \rangle_Q, \tag{17}$$

and invoking the corrector equation (3) for ξ^*, we observe that this term is actually zero. Thus, Equation (16) may be written

$$\langle (\varepsilon - \varepsilon^*) : \mathbb{C} : (\xi - \xi^*) \rangle_Q = \langle (\varepsilon - \varepsilon^*) : \mathbb{C} : \xi \rangle_Q = \langle \varepsilon : \mathbb{C} : \xi \rangle_Q - \langle \varepsilon^* : \mathbb{C} : \xi \rangle_Q. \tag{18}$$

The last term may be transformed into

$$
\begin{aligned}
\langle \varepsilon^* : \mathbb{C} : \xi \rangle_Q &= \langle \xi : \mathbb{C} : \varepsilon^* \rangle_Q \\
&= \left\langle (\overline{\xi} + \nabla^s v) : \mathbb{C} : \varepsilon^* \right\rangle_Q \\
&= \left\langle \overline{\xi} : \mathbb{C} : \varepsilon^* \right\rangle_Q + \langle \nabla^s v : \mathbb{C} : \varepsilon^* \rangle_Q \\
&= \overline{\xi} : \langle \mathbb{C} : \varepsilon^* \rangle_Q \\
&= \overline{\xi} : \mathbb{C}^{\texttt{eff}} : \overline{\varepsilon},
\end{aligned}
\tag{19}
$$

where we used the form (12) of ξ, the fact that the corrector equation (3) holds for ε^* and the definition (6) of the effective stiffness. Inserting the latter expression into Equation (18) completes the derivation of the identity (13). We conclude with a few remarks.

1. We only presumed that the local stiffnesses $\mathbb{C}(x)$ are positive semidefinite in order to include porous materials. In a way, the uniqueness of solutions is used implicitly in the definition of the effective stiffness (6) and also in the accuracy estimates. Such uniqueness may be obtained for porous materials if the interface between the solid and the gaseous material is not too rough, see Schneider.[37]
2. The present discussion centered on the continuous case, that is, the non-discretized corrector equation (3). The theory, however, generalizes viz-a-viz to discretizations of the balance Equation (3) that are based on the displacement and whose divergence operators are (negative) adjoints of the symmetrized gradient operators. This is the case for Fourier-type,[23,24,43-45] finite-difference,[46-49] and finite-element[50-53] discretizations used in FFT-based computational micromechanics.
3. The identity (13) is commonly used when analyzing the convergence of Galerkin methods upon mesh refinement,[27,54,55] that is, where the fields ε and ξ live in an appropriate subspace. In contrast, we use the associated bound (14) for improving numerical estimates for the effective elastic moduli and a *fixed* discretization (both in terms of the type and the mesh level).

3 | CONSEQUENCES FOR POSTPROCESSING SOLUTION METHODS

In this section, we demonstrate how the theory developed in Section 2 may be applied to solution methods used in computational homogenization. For this purpose, let us detail on how the effective stiffness is typically calculated in computational homogenization. First, select an orthonormal basis $e_1, \dots, e_{d(d+1)/2}$ of the space $\text{Sym}(d)$ of symmetric $d \times d$ tensors, that is, which satisfy

$$
e_i : e_j = \begin{cases} 1, & i = j, \\ 0, & \text{otherwise}, \end{cases} \quad i, j = 1, \dots, d(d+1)/2.
\tag{20}
$$

Then, compute approximate solutions $\varepsilon_i = e_i + \nabla^s v_i$ to the corrector equation (3) with $\overline{\varepsilon} = e_i$. Once the approximate solutions are computed, the effective stiffness is approximated column-wise via

$$
\mathbb{C}^{\texttt{eff,strain}} : e_i \equiv \langle \mathbb{C} : \varepsilon_i \rangle_Q,
\tag{21}
$$

when using strain equivalence. In contrast, the effective stiffness may be estimated entry-by-entry

$$
e_j : \mathbb{C}^{\texttt{eff,energy}} : e_i \equiv \left\langle \varepsilon_j : \mathbb{C} : \varepsilon_i \right\rangle_Q,
\tag{22}
$$

via the energy equivalence principle. Both approaches are summarized in Algorithms 1 and 2.

Algorithm 1. Elastic homogenization by strain equivalence

1: **for** $i = 1, \ldots, d(d+1)/2$ **do**
2:     solve Equation (3) for $\bar{\varepsilon} = e_i$ with result ε_i
3: **end for**
4: Compute effective stiffness $\mathbb{C}^{\mathrm{eff,strain}}$ by $\mathbb{C}^{\mathrm{eff,strain}} : e_i \equiv \langle \mathbb{C} : \varepsilon_i \rangle_Q$ column-wise

---

Algorithm 2. Elastic homogenization by energy equivalence

1: **for** $i = 1, \ldots, d(d+1)/2$ **do**
2:     solve Equation (3) for $\bar{\varepsilon} = e_i$ with result ε_i
3: **end for**
4: Compute effective stiffness $\mathbb{C}^{\mathrm{eff,energy}}$ by $e_j : \mathbb{C}^{\mathrm{eff,energy}} : e_i \equiv \langle \varepsilon_j : \mathbb{C} : \varepsilon_i \rangle_Q$ entry-wise

---

Suppose that a numerical solution method is used with a convergence rate encoded by a contraction factor $\rho \in (0, 1)$, that is, for chosen initial guesses ε_i^0, the iterates ε_i^k approach the solution ε_i^* of the corrector equation (3) satisfying the inequality

$$\| \varepsilon_i^k - \varepsilon_i^* \|_{L^2} \leq C \, \rho^k \, \| \varepsilon_i^0 - \varepsilon_i^* \|_{L^2} \tag{23}$$

with a constant C only depending on the stiffness distribution $\mathbb{C}$ and the solution method. Suppose that we always use k iterations to compute the approximate solution ε_i^k for any macroscopic loading e_i. Then, the estimate (9) applied to the strain equivalence (21) yields

$$\left\| \mathbb{C}^{\mathrm{eff,strain}} : e_i - \mathbb{C}^{\mathrm{eff}} : e_i \right\| \leq L \, \| \varepsilon_i^k - \varepsilon_i^* \|_{L^2} \leq LC \, \| \varepsilon_i^0 - \varepsilon_i^* \|_{L^2} \, \rho^k. \tag{24}$$

In turn, the estimate (14) applied to the effective stiffness computed via energy equivalence gives

$$\left| e_j : \mathbb{C}^{\mathrm{eff,energy}} : e_i - e_j : \mathbb{C}^{\mathrm{eff}} : e_i \right| \leq LC^2 \, \| \varepsilon_i^0 - \varepsilon_i^* \|_{L^2} \| \varepsilon_j^0 - \varepsilon_j^* \|_{L^2} \, \rho^{2k}. \tag{25}$$

Thus, the using energy equivalence produces an effective stiffness which converges twice as fast as using strain equivalence.

Both inequalities (24) and (25) are estimates, that is, they may be too pessimistic, and involve unknown constants, that is, the distance to the solution. Thus, we investigate a computational example to assess the sharpness of the estimates. For this purpose, we investigate Moulinec–Suquet's basic scheme[23,24]

$$\varepsilon^{k+1} = \bar{\varepsilon} - \Gamma^0 : (\mathbb{C} - \mathbb{C}^0) : \varepsilon^k, \tag{26}$$

for solving the corrector equation (3). Here, $\mathbb{C}^0$ is the reference material and $\Gamma^0 = \nabla^s (\mathrm{div}\, \mathbb{C}^0 : \nabla^s)^\dagger \mathrm{div}$ denotes the associated Green's operator. We utilize the original Moulinec–Suquet discretization[23,24] and investigate a single spherical glass inclusion at 12.9% volume fraction, see Figure 1A, in a polypropylene matrix with linear elastic material properties shown in Table 1. We consider a reference material proportional to the identity, whose proportionality constant is set to the average of the minimum and maximum eigenvalues of the microscopic stiffnesses considered, and measure convergence with the criterion

$$\mathrm{residual}^k \equiv \frac{\| \mathbb{C}^0 : \Gamma^0 : \mathbb{C} : \varepsilon^k \|_{L^2}}{\langle \mathbb{C} : \varepsilon^k \rangle_Q} \overset{!}{\leq} \mathrm{tol}, \tag{27}$$

which is proportional to the distance to the solution, yet computable. For a 32^3-microstructure and $\bar{\varepsilon} = 0.01 \, e_1 \otimes e_1$, the convergence rates of various quantities are compared in Figure 2A. As the reference for the effective stresses, we take the result of the conjugate gradient method solved up to a tolerance $\mathrm{tol} = 10^{-14}$. We observe that the effective
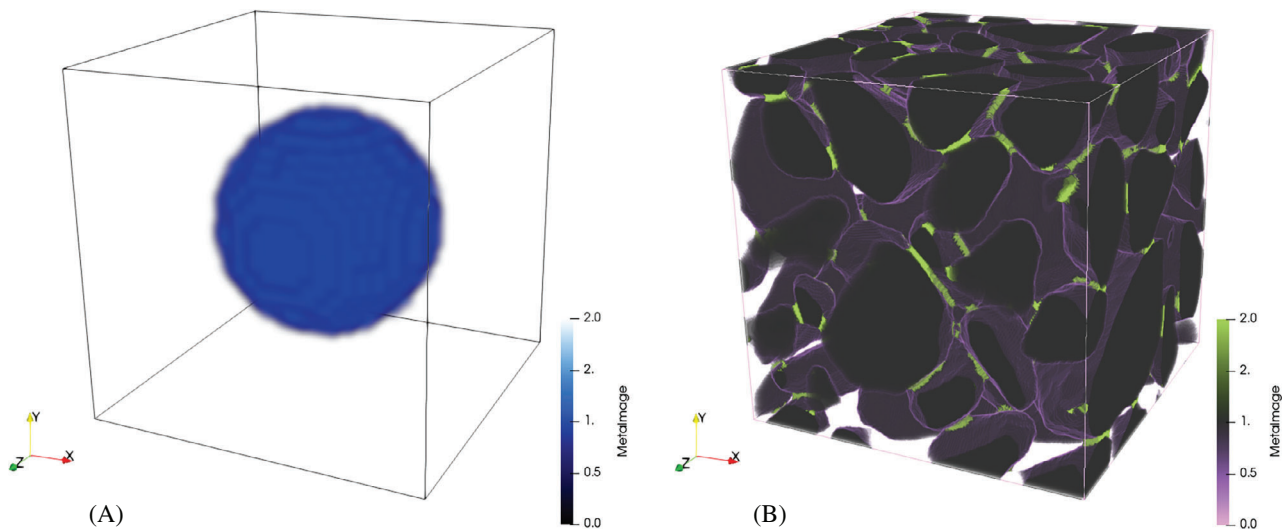
FIGURE 1 Microstructures considered in this article. (A) Spherical inclusion at 12.9% volume, 32^3 voxels; (B) Digital sandcore,[56] 256^3 voxels

TABLE 1 Material parameters used in this article, supplemented by their source.

Material	E in GPa	v
E-glass inclusion[57]	72	0.22
Polymer matrix[57]	2.1	0.3
Quartz sand grains[58,59]	66.9	0.25
Quartz glass binder[60]	71.7	0.17

stresses computed by the strain equivalence principle (21) converge with the same rate as the residual. This observation agrees with the theoretical prediction (24). Furthermore, Figure 2A reveals that the effective stress computed by energy equivalence (22) converges with twice the rate, conforming to theory (25).

Interestingly, this type of higher accuracy also continues to hold for solvers extending the basic scheme, as long as each iterate satisfies kinematic compatibility. As an example of a solution method without monotone convergence we consider Nesterov's method,[61,62] introduced into FFT-based computational homogenization in the work.[63] In Figure 2B, we observe that the effective properties computed by strain equivalence are much more prone to fluctuations than the results postprocessed through energy equivalence. Moreover, the latter are consistently more accurate than the former, again following the square of the residual closely.

For both considered examples shown in Figure 2 that, for a fixed accuracy, only half of the iterations are required for energy equivalence than for strain equivalence.

The golden standard for solving linear problems with symmetric and positive definite linear operator is the conjugate gradient method,[25] which was proposed in the context of FFT-based micromechanics by Brisard and Dormieux[27] and Zeman et al.[26] Applied to the same problem as before, Figure 2C shows that something interesting is happening. In fact, five of the six stress components converge with the same rate as the residual. In Figure 2C, only the yy-component is shown. However, the xx-component of the stress, the one aligned with the macroscopic direction of strain, converges with double rate when computed by strain equivalence. Thus, it appears that working with energy equivalence is not strictly necessary for the CG method, at least provided only the quantity

$$\bar{\varepsilon} : \langle \mathbb{C} : \varepsilon \rangle_Q,$$ (28)

is of interest. In fact, for the standard implementation of the CG method (with an initial guess of $\varepsilon^0 \equiv \bar{\varepsilon}$), the identity

$$\bar{\varepsilon} : \langle \mathbb{C} : \varepsilon^{k+1} \rangle_Q = \langle \varepsilon^k : \mathbb{C} : \varepsilon^{k+1} \rangle_Q,$$ (29)
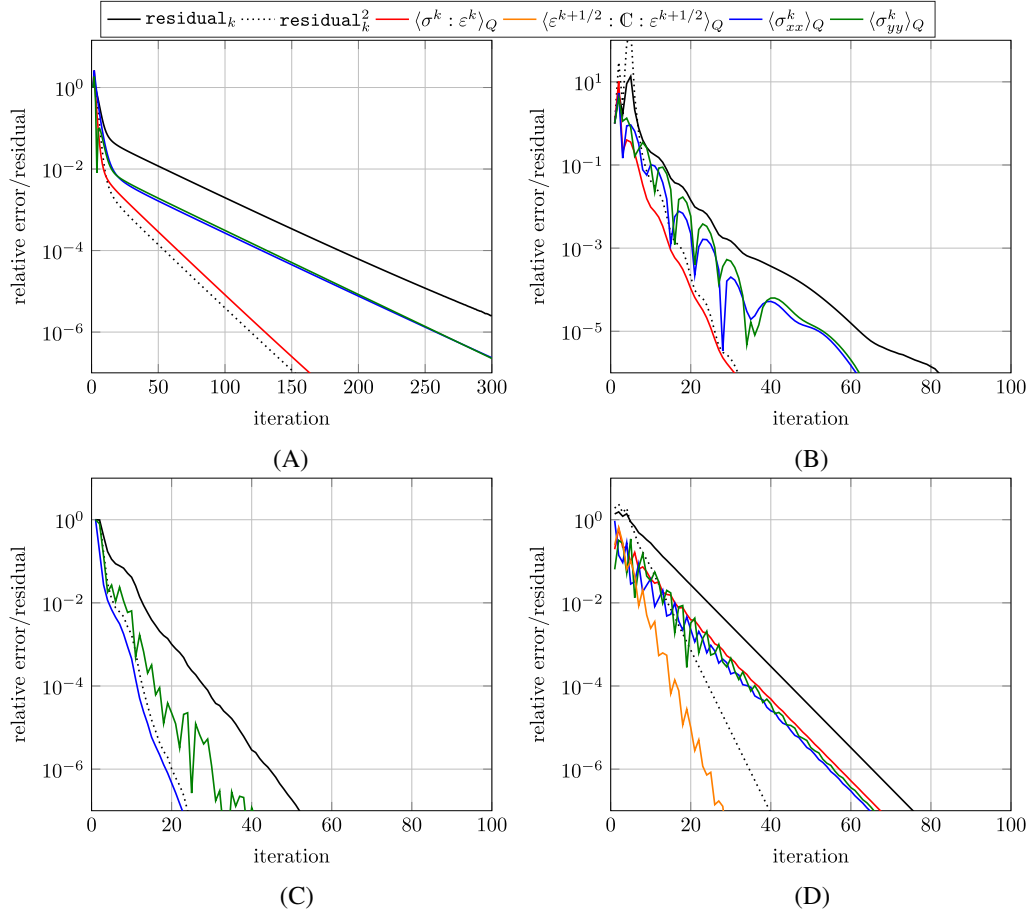
FIGURE 2 Comparison of different averaging methods for estimating the effective properties compared to the residual (27) for various solvers and the single-inclusion microstructure, see Figure 1A. (A) Basic scheme; (B) Nesterov's method; (C) CG; (D) ADMM with $\gamma = 0$

can be shown for each iteration index $k \geq 0$. In particular, strain-equivalence type averaging in macroscopic loading direction actually emulates energy equivalence when using CG. In particular, in view of r-linear convergence of the form (23), we obtain

$$\left| \overline{\varepsilon} : \left\langle \mathbb{C} : \varepsilon^{k+1} \right\rangle_Q - \overline{\varepsilon} : \mathbb{C}^{\text{eff}} : \overline{\varepsilon} \right| \leq L C^2 \left\| \varepsilon^0 - \varepsilon^* \right\|^2 \rho^{2k+1}, \tag{30}$$

that is, convergence with the double rate. In fact, these considerations provide an insight into the CG method and show that some components of the stress converge much faster than others. In particular, extra accuracy is provided in the direction of interest by CG automatically.

The identity (29) may be shown exploiting the various orthogonality properties of CG, see Appendix A. When deriving the identity (13), the compatibility of (at least one of) the test fields ε and ξ was essential. To check whether this condition is actually necessary we investigate the ADMM iterative scheme

$$\varepsilon^{k+\frac{1}{2}} = \overline{\varepsilon} - \Gamma^0 : (\sigma^k - \mathbb{C}^0 : e^k),$$
$$\varepsilon^{k+1} = 2(1 - \gamma)\varepsilon^{k+\frac{1}{2}} - (1 - 2\gamma)e^k,$$
$$(\mathbb{C} + \mathbb{C}^0) : e^{k+1} = \sigma^k + \mathbb{C}^0 : \varepsilon^{k+1},$$
$$\sigma^{k+1} = \sigma^k + \mathbb{C}^0 : (\varepsilon^{k+1} - e^{k+1}), \tag{31}$$

specialized to linear elasticity, initialized by

$$e^0 \equiv \varepsilon^0 \quad \text{and} \quad \sigma^0 = \mathbb{C} : \varepsilon^0, \tag{32}$$

for prescribed ε^0. For $\gamma = 1/2$, the method (31) was introduced into the FFT community by Michel et al.[64,65] under the name *accelerated scheme*. For general $\gamma \in [0, 1)$, the method (31) was considered by Monchiet and Bonnet.[66,67] Moulinec and Silva[68] pointed out that, for $\gamma = 0$, the iterative scheme (31) coincides with the polarization-based algorithm introduced by Eyre and Milton.[69]

The iterative scheme (31) involves three strain fields, $\varepsilon^{k+1/2}$, ε^k, and e^k, and a stress field σ^k. The strain field $\varepsilon^{k+1/2}$ is always compatible (provided ε^0 is compatible), whereas the fields e^k and σ^k are always related by the constitutive law, that is, Hooke's law

$$\sigma^k = \mathbb{C} : e^k. \tag{33}$$

Only upon convergence, the field e^k becomes compatible (as all three strain fields coincide). In Figure 2D, the convergence behavior of ADMM with $\gamma = 0$ is shown, together with online estimates of the averaged stresses in x- and y-direction as well as the energy

$$\left\langle \varepsilon^k : \sigma^k \right\rangle_Q. \tag{34}$$

We observe a rather fast convergence of the residual. The estimates for the stress, obtained both by strain and by energy equivalence, do converge at the same rate. Thus, incompatible test fields cannot profit from the increased accuracy provided by the fundamental identity (13), which presupposes compatibility. Rather, it appears advantageous to work with the compatible field $\varepsilon^{k+1/2}$ instead. To investigate this idea, we computed, in addition, the energy

$$\left\langle \varepsilon^{k+1/2} : \mathbb{C} : \varepsilon^{k+1/2} \right\rangle_Q, \tag{35}$$

highlighted in orange in Figure 2D. It turns out that the energy (35) is not only consistently more accurate than the naive version (34), but also converges at a higher rate, as predicted by our theory. In particular, when polarization schemes are used for solving the corrector equation (3), the effective elastic properties of a composite should be computed by energy equivalence with the field $\varepsilon^{k+1/2}$, dispensing with the fields ε^k, e^k, and σ^k! If an implementation on the polarization is used, see Schneider et al.[70] for details, the final polarization field P^k should be postprocessed to the field

$$\varepsilon^{k+1/2} = \overline{\varepsilon} + \Gamma^0 : (\mathbb{C} - \mathbb{C}^0)(\mathbb{C} + \mathbb{C}^0)^{-1} : P^k,$$

serving as the basis for strain equivalence.

Next, we consider a more complex material. More precisely, we look at a sand core microstructure,[56] see Figure 1B, composed of individual sand grains (dark) bound together by an anorganic binder (green). The microstructure consists of three phases: the sand grains, about 1%-vol of binder and the remaining about 40% of pore space. We use the staggered grid discretization[47] due to its advantages for porous materials,[37] rely upon the material parameters listed in Table 1 and subject the composite to a strain of $\overline{\varepsilon} = 0.01 \, e_1 \otimes e_1$. The performance of the individual solvers and the stiffness-extraction schemes are shown in Figure 3. The basic scheme, see Figure 3A, converges rather slowly. The averaged stresses converge at a similar rate, with an exception for the transverse stress σ_{yy} roughly at iteration 450. The stress obtained through energy equivalence converges faster and is more than one order of magnitude more accurate than the strain-equivalence results. Although the basic scheme is not competitive in terms of residual versus runtime, it would still be possible to extract sufficiently accurate effective properties in reasonable time through energy equivalence.

As the second solver we consider Nesterov's method, this time with speed restart.[71] This setup is necessary for porous materials and the inherent infinite material contrast, as the theoretically optimal damping coefficient degenerates to unity in this case (which is clearly not optimal). In Figure 3B, we observe a similar behavior as for the basic scheme, but with non-monotonic convergence behavior.

Taking a look at the conjugate gradient method, see Figure 3C, we see that the transverse stress σ_{yy} converges with the same rate as the residual, whereas the axial stress σ_{xx} obtained through strain equivalence, converges with the double rate. This again confirms the theoretical developments in Appendix A.

Last but not least, we take a look at ADMM (31) with $\gamma = 1/4$ and an adaptive selection of the reference material, the Lorenz and Tran-Dinh scaling,[72] which turned out to perform best among several studied choices.[73] We observe that the stresses computed either by strain or by energy equivalence (34) all converge at the same rate which is moreover proportional to the convergence criterion. However, for this scenario and after about 100 iterations, energy equivalence produces
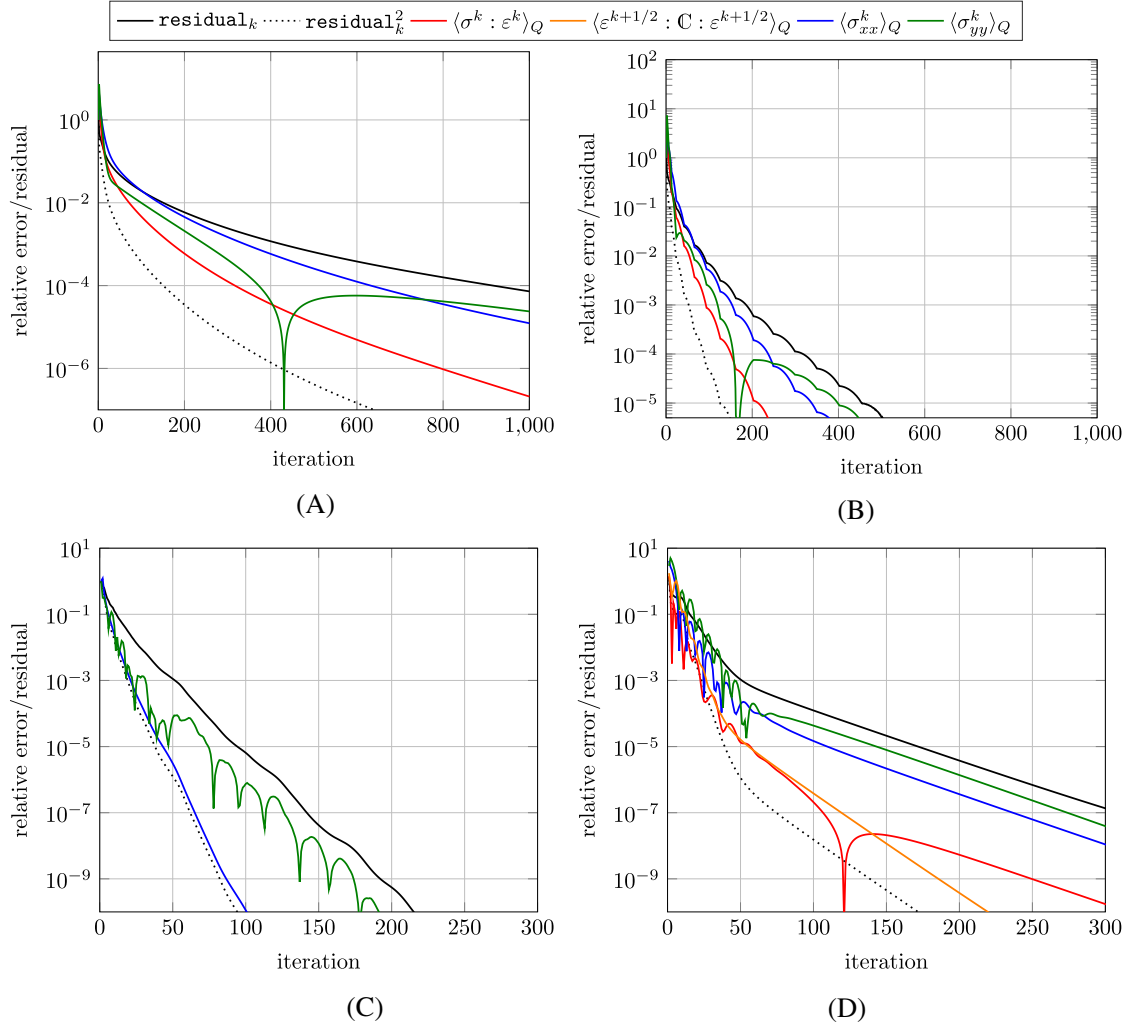
FIGURE 3 Comparison of different averaging methods for estimating the effective properties compared to the residual (27) for various solvers and the sandcore microstructure, see Figure 1B. (A) Basic scheme; (B) Nesterov's method; (C) CG; (D) ADMM with $\gamma = 1/4$

results that are between one and two orders of magnitude more accurate than those obtained through strain equivalence. Even more powerful is using the improved estimate (35) based on the iterate $\varepsilon^{k+1/2}$, as it features a convergence rate that is twice as high as the other averaging possibilities.

4 | CONCLUSION

This work was devoted to improving the calculated effective linear elastic properties of composites through averaging the elastic energy rather than the stress field. We worked with periodic boundary conditions, although other boundary conditions do work as long as an appropriate integration by parts is available, classically encoded by the validity of the Hill–Mandel condition.

We could show that the accuracy is roughly doubled when the energy equivalence is used rather than strain equivalence. Moreover, we discussed how to take advantage of these ideas also for polarization methods which come with non-compatible iterates. Last but not least, we showed that a specific component of the averaged stress does indeed converge as if energy equivalence was used for iterates of the linear conjugate gradient method.

In retrospect, the difference between the two averaging schemes does not come as a surprise. For instance, the identity

$$\|\mathbb{C}^0 : \Gamma^0 : \mathbb{C} : \varepsilon^k\|_{L^2} = \left\langle \varepsilon^{k+1} : \mathbb{C}^0 : \varepsilon^{k+1} \right\rangle_Q - \left\langle \varepsilon^k : \mathbb{C}^0 : \varepsilon^k \right\rangle_Q - 2\left(\left\langle \varepsilon^k : \mathbb{C} : \varepsilon^k \right\rangle_Q - \overline{\varepsilon} : \left\langle \mathbb{C} : \varepsilon^k \right\rangle_Q \right), \quad (36)$$

provided by Ernesti et al.[74(eq. 3.6)] expresses the residual (27) of the basic scheme as the difference of elastic energies of subsequent iterates and the failure to satisfy the Hill–Mandel condition.[75,76] Clearly, over the last decades computational micromechanics has developed significantly, moving beyond linear elasticity despite its central importance. Thus, it is imperative to understand whether a strategy similar to energy equivalence is also feasible to work for constitutive laws that are inelastic. Perhaps the simplest such example concerns thermal eigenstrains $\alpha(x)$, prescribed at each microscopic point $x \in Q$. The effective eigenstress $\overline{\sigma}$ computes via

$$\overline{\sigma} = \langle \mathbb{C} : \xi^* \rangle_Q, \quad \text{where the stress associated to} \quad \xi^* = \nabla^s v^* - \alpha, \tag{37}$$

is in equilibrium. The classical Mandel–Levin formula[77,78] allows one to bypass computing ξ^*, as long as the correctors ε_i^* corresponding to the macroscopic loads e_i are available through the expression

$$e_i : \overline{\sigma} = \left\langle \varepsilon_i^* : \mathbb{C} : \alpha \right\rangle_Q. \tag{38}$$

Clearly, if the correctors ε_i are only computed with finite precision, the estimate

$$\langle \varepsilon_i : \mathbb{C} : \alpha \rangle_Q - e_i : \overline{\sigma} = O(\|\varepsilon_i - \varepsilon_i^*\|_{L^2}), \tag{39}$$

will be sharp, in general, and no superaccuracy can be reached. Instead, if a further approximation ξ to the corrector ξ^* is available, an estimate

$$\langle \varepsilon_i : \mathbb{C} : \xi \rangle_Q - e_i : \overline{\sigma} = O(\|\varepsilon_i - \varepsilon_i^*\|_{L^2} \|\xi - \xi^*\|_{L^2}), \tag{40}$$

follows. This means, on the other hand, that—in three spatial dimensions—an additional *seventh* corrector problem needs to be solved. Thus, to reach a prescribed accuracy acc, instead of solving six problems to acc, seven problems need to be solved to acc/2. Thus, when thermal eigenstresses are of interest, the effort is only reduced by 41.$\overline{6}$% through energy equivalence.

Things get even more complicated for general non-linear constitutive laws. For such a scenario, the field ε_i in the estimate (40) should be replaced by a corresponding linearized corrector.[79] Depending on the effort involved in evaluating the nonlinear constitutive law, it may be advantageous to spend time computing the (six) tangent correctors instead of computing the single (nonlinear) corrector field to high accuracy. Similarly, it would be of interest to investigate whether an extension to finite strains is possible.

DATA AVAILABILITY STATEMENT
The data that support the findings of this study are available from the corresponding author upon reasonable request.

ENDNOTE
*Throughout the article, the terms effective and apparent are not distinguished in the main text. Rather, the term effective property is also used for the apparent property of the cell.

ORCID
Matti Schneider https://orcid.org/0000-0001-7017-3618

REFERENCES
1. Matouš K, Geers MGD, Kouznetsova VG, Gillman A. A review of predictive nonlinear theories for multiscale modeling of heterogeneous materials. *J Comput Phys.* 2017;330:192-220.
2. Kozlov SM. Averaging of differential operators with almost periodic rapidly oscillating coefficients. *Math USSR-Sbornik.* 1978;107(2):199-217.

3. Papanicolaou GC, Varadhan SRS. Boundary value problems with rapidly oscillating random coefficients. In: Bolyai J, ed. *Random Fields, Vol. I, II (Esztergom, 1979), Volume 27 of Colloquia Mathematica Societatis.* North-Holland; 1981:835-873.

4. Hill R. Elastic properties of reinforced solids: some theoretical principles. *J Mech Phys Solids.* 1963;11(5):357-372.

5. Drugan WJ, Willis JR. A micromechanics-based nonlocal constitutive equations and estimates of representative volume element size for elastic composites. *J Mech Phys Solids.* 1996;44:497-524.

6. Kanit T, Forest S, Galliet I, Mounoury V, Jeulin D. Determination of the size of the representative volume element for random composites: statistical and numerical approach. *Int J Solids Struct.* 2003;40(13–14):3647-3679.

7. Gloria A, Otto F. An optimal variance estimate in stochastic homogenization of discrete elliptic equations. *Ann Probab.* 2011;39(3):779-856.

8. Ostoja-Starzewski M, Schulte J. Bounding of effective thermal conductivities of multiscale materials by essential and natural boundary conditions. *Phys Rev B.* 1996;54(1):278.

9. Bourgeat A, Piatnitski A. Approximations of effective coefficients in stochastic homogenization. *Annales de l'Intitut H Poincaré.* 2004;40:153-165.

10. Yue X, Weinan E. The local microscale problem in the multiscale modeling of strongly heterogeneous media: effects of boundary conditions and cell size. *J Comput Phys.* 2007;222(2):556-572.

11. Sab K. On the homogenization and the simulation of random materials. *Eur J Mech A/Solids.* 1992;11:585-607.

12. Sab K, Nedjar B. Periodization of random media and representative volume element size for linear composites. *C R Mécanique.* 2005;333(2):187-195.

13. Schneider M, Josien M, Otto F. Representative volume elements for matrix-inclusion composites - a computational study on the effects of an improper treatment of particles intersecting the boundary and the benefits of periodizing the ensemble. *J Mech Phys Solids.* 2022;158:104652.

14. Abdylle A, Weinan E. Finite difference heterogeneous multi-scale method for homogenization problems. *J Comput Phys.* 2003;191(1):18-39.

15. Yvonnet J. *Computational Homogenization of Heterogeneous Materials with Finite Elements.* Solid Mechanics and Its Applications. Vol 258. Springer; 2019.

16. Cavalcante MAA, Pindera M-J, Khatam H. Finite-volume micromechanics of periodic materials: past, present and future. *Compos Part B.* 2012;43(6):2521-2543.

17. Owen SJ, Brown JA, Ernst CD, Lim H, Long KN. Hexahedral mesh generation for computational materials modeling. *Proc Eng.* 2017;203:167-179.

18. Landis EN, Keane DT. X-ray microtomography. *Mater Char.* 2010;61:1305-1316.

19. Guven I, Cinar K. Micromechanical modeling of particulate-filled composites using micro-CT to create representative volume elements. *Int J Mech Mater Des.* 2019;15:695-714.

20. Keyak J, Meagher J, Skinner H, Motejr C. Automated three-dimensional finite element modelling of bone: a new method. *Biotechnol Bioeng.* 1990;12(5):389-397.

21. Hollister SJ, Kikuchi N. Homogenization theory and digital imaging: a basis for studying the mechanics and design principles of bone tissue. *Biotechnol Bioeng.* 2017;43(7):586-596.

22. Mishnaevsky L. Automatic voxel-based generation of 3D microstructural FE models and its application to the damage analysis of composites. *Mater Sci Eng A.* 2005;407(1–2):11-23.

23. Moulinec H, Suquet P. A fast numerical method for computing the linear and nonlinear mechanical properties of composites. *Comptes Rendus de l'Académie des Sciences Série II.* 1994;318(11):1417-1423.

24. Moulinec H, Suquet P. A numerical method for computing the overall response of nonlinear composites with complex microstructure. *Comput Methods Appl Mech Eng.* 1998;157:69-94.

25. Hestenes M, Stiefel E. Methods of conjugate gradients for solving linear systems. *J Res Natl Bur Stand.* 1952;49:409-436.

26. Zeman J, Vondřejc J, Novák J, Marek I. Accelerating a FFT-based solver for numerical homogenization of periodic media by conjugate gradients. *J Comput Phys.* 2010;229(21):8065-8071.

27. Brisard S, Dormieux L. FFT-based methods for the mechanics of composites: a general variational framework. *Comput Mater Sci.* 2010;49(3):663-671.

28. Gélébart L, Mondon-Cancel R. Non-linear extension of FFT-based methods accelerated by conjugate gradients to evaluate the mechanical behavior of composite materials. *Comput Mater Sci.* 2013;77:430-439.

29. Kabel M, Böhlke T, Schneider M. Efficient fixed point and Newton-Krylov solvers for FFT-based homogenization of elasticity at large deformations. *Comput Mech.* 2014;54(6):1497-1514.

30. Lebensohn RA, Rollett AD. Spectral methods for full-field micromechanical modelling of polycrystalline material. *Comput Mater Sci.* 2020;173:109336.

31. Segurado J, Lebensohn RA, Lorca J. Ch. 1. Computational homogenization of polycrystals. *Adv Appl Mech.* 2018;51:1-114.

32. Schneider M. A review of non-linear FFT-based computational homogenization methods. *Acta Mech.* 2021;232:2051-2100.

33. Lucarini S, Upadhyay MV, Segurado J. FFT based approaches in micromechanics: fundamentals, methods and applications. *Model Simul Mater Sci Eng.* 2022;30(2):023002.

34. Zeller R, Dederichs PH. Elastic constants of polycrystals. *Phys Status Solidi.* 1973;55(2):831-842.

35. Kröner E. Bounds for effective elastic moduli of disordered materials. *J Mech Phys Solids.* 1977;25(2):137-155.

36. Mura T. *Micromechanics of Defects in Solids.* Martinus Nijhoff; 1987.

37. Schneider M. Lippmann-Schwinger solvers for the computational homogenization of materials with pores. *Int J Numer Methods Eng*. 2020;121(22):5017-5041.

38. Ye C, Chung ET. Numerical analysis of several FFT-based schemes for computational homogenization; 2022. arXiv preprint arXiv:2201.01916

39. Bellis C, Moulinec H, Suquet P. Eigendecomposition-based convergence analysis of the Neumann series for laminated composites and discretization error estimation. *Int J Nume Methods Eng*. 2020;121:201-232.

40. Liu Z, Wu CT, Koishi M. A deep material network for multiscale topology learning and accelerated nonlinear modeling of heterogeneous materials. *Comput Methods Appl Mech Eng*. 2019;345:1138-1168.

41. Gajek S, Schneider M, Böhlke T. On the micromechanics of deep material networks. *J Math Phys Solids*. 2020;142:103984.

42. Wriggers P, Zohdi TI. *An Introduction to Computational Micromechanics*. Lecture Notes in Applied and Computational Mechanics. Springer; 2008.

43. Bonnet G. Effective properties of elastic periodic composite media with fibers. *J Mech Phys Solids*. 2007;55:881-899.

44. Vondřejc J, Zeman J, Marek I. Guaranteed upper-lower bounds on homogenized properties by FFT-based Galerkin method. *Comput Methods Appl Mech Eng*. 2015;297:258-291.

45. Monchiet V. Combining FFT methods and standard variational principles to compute bounds and estimates for the properties of elastic composites. *Comput Methods Appl Mech Eng*. 2015;283:454-473.

46. Willot F. Fourier-based schemes for computing the mechanical response of composites with accurate local fields. *C R Mécanique*. 2015;343:232-245.

47. Schneider M, Ospald F, Kabel M. Computational homogenization of elasticity on a staggered grid. *Int J Numer Methods Eng*. 2016;105(9):693-720.

48. Vidyasagar A, Tan WL, Kochmann DM. Predicting the effective response of bulk polycrystalline ferroelectric ceramics via improved spectral phase field methods. *Mech Phys Solids*. 2017;106:133-151.

49. Vidyasagar A, Tutcuoglu AD, Kochmann DM. Deformation patterning in finite-strain crystal plasticity by spectral homogenization with application to magnesium. *Comput Methods Appl Mech Eng*. 2018;335:584-609.

50. Schneider M, Merkert D, Kabel M. FFT-based homogenization for microstructures discretized by linear hexahedral elements. *Int J Numer Methods Eng*. 2017;109:1461-1489.

51. Brisard S. Reconstructing displacements from the solution to the periodic Lippmann-Schwinger equation discretized on a uniform grid. *Int J Numer Methods Eng*. 2017;109(4):459-486.

52. Leuschner M, Fritzen F. Fourier-accelerated nodal solvers (FANS) for homogenization problems. *Comput Mech*. 2018;62: 359-392.

53. Leute RJ, Ladecký M, Falsafi A, et al. Elimination of ringing artifacts by finite-element projection in FFT-based homogenization. *J Comput Phys*. 2022;453:110931.

54. Brisard S, Dormieux L. Combining Galerkin approximation techniques with the principle of Hashin and Shtrikman to derive a new FFT-based numerical method for the homogenization of composites. *Comput Methods Appl Mech Eng*. 2012;217 – 220:197-212.

55. Schneider M. Convergence of FFT-based homogenization for strongly heterogeneous media. *Math Methods Appl Sci*. 2015;38(13):2761-2778.

56. Schneider M, Hofmann T, Andrä H, et al. Modeling the microstructure and computing effective elastic properties of sand core materials. *Int J Solids Struct*. 2018;143:1-17.

57. Wu L, Adam L, Doghri I, Noels L. An incremental-secant mean-field homogenization method with second statistical moments for elasto-visco-plastic composite materials. *Mech Mater*. 2017;114:180-200.

58. Daphalapurkar NP, Wang F, Fu B, Lu H, Komanduri R. Determination of mechanical properties of sand grains by nanoindentation. *Exp Mech*. 2011;51:719-728.

59. Wichtmann T, Triantafyllidis T. On the influence of the grain size distribution curve on P-wave velocity, constrained elastic modulus M_{max} and Poisson's ratio of quartz sands. *Soil Dyn Earthq Eng*. 2010;30(8):757-766.

60. Sanditov DS, Mantatov VV, Sanditov BD. Poisson ratio and plasticity of glasses. *Tech Phys*. 2009;54(4):594-596.

61. Nesterov Y. A method for solving the convex programming problem with convergence rate $O\left(1/k^2\right)$. *Dokladi Akademii Nauk SSSR*. 1983;269(3):543-547.

62. Nesterov Y. *Introductory Lectures on Convex Optimization: A Basic Course*. Mathematics and Its Applications. Kluwer Academic Publishers; 2004.

63. Schneider M. An FFT-based fast gradient method for elastic and inelastic unit cell homogenization problems. *Comput Methods Appl Mech Eng*. 2017;315:846-866.

64. Michel JC, Moulinec H, Suquet P. A computational method based on augmented Lagrangians and fast Fourier transforms for composites with high contrast. *Comput Model Eng Sci*. 2000;1(2):79-88.

65. Michel JC, Moulinec H, Suquet P. A computational scheme for linear and non-linear composites with arbitrary phase contrast. *Int J Numer Methods Eng*. 2001;52:139-160.

66. Monchiet V, Bonnet G. A polarization-based FFT iterative scheme for computing the effective properties of elastic composites with arbitrary contrast. *Int J Numer Methods Eng*. 2012;89:1419-1436.

67. Monchiet V, Bonnet G. Numerical homogenization of nonlinear composites with a polarization-based FFT iterative scheme. *Comput Mater Sci*. 2013;79:276-283.

68. Moulinec H, Silva F. Comparison of three accelerated FFT-based schemes for computing the mechanical response of composite materials. *Int J Numer Methods Eng.* 2014;97:960-985.

69. Eyre DJ, Milton GW. A fast numerical scheme for computing the response of composites using grid refinement. *Eur Phys J Appl Phys.* 1999;6(1):41-47.

70. Schneider M, Wicht D, Böhlke T. On polarization-based schemes for the FFT-based computational homogenization of inelastic materials. *Comput Mech.* 2019;64(4):1073-1095.

71. Su W, Boyd S, Candes E. A differential equation for modeling Nesterov's accelerated gradient method: theory and insights. In: Ghahramani Z, Welling M, Cortes C, Lawrence ND, Weinberger KQ, eds. *Advances in Neural Information Processing Systems.* Vol 27. Curran Associates, Inc.; 2014:2510-2518.

72. Lorenz DA, Tran-Dinh Q. Non-stationary Douglas–Rachford and alternating direction method of multipliers: adaptive step-sizes and convergence. *Comput Optim Appl.* 2019;74:67-92.

73. Schneider M. On non-stationary polarization methods in FFT-based computational micromechanics. *Int J Numer Methods Eng.* 2021;122(22):6800-6821.

74. Ernesti F, Schneider M, Böhlke T. Fast implicit solvers for phase field fracture problems on heterogeneous microstructures. *Comput Methods Appl Mech Eng.* 2020;363:112793.

75. Hill R. On constitutive macro-variables for heterogeneous solids at finite strain. *Proc Royal Soc Lond A Math Phys Sci.* 1972;326(1565):131-147.

76. Mandel J. *Plasticité classique et viscoplasticité.* Springer; 1972.

77. Mandel J. Generalisation de la theorie de plasticite de W. T. Koiter. *Int J Solids Struct.* 1965;1(3):273-295.

78. Levin VM. On the coefficients of thermal expansion of heterogeneous materials. *Mech Solids.* 1967;2:58-61.

79. Fischer J, Neukamm S. Optimal homogenization rates in stochastic homogenization of nonlinear uniformly elliptic equations and systems. *Arch Ration Mech Anal.* 2021;242:343-452.

80. Nocedal J, Wright SJ. *Numerical Optimization.* Springer; 1999.

81. Kabel M, Andrä H. Fast numerical computation of precise bounds of effective elastic moduli. *Berichte des Fraunhofer ITWM.* 2013;224:1-16.

APPENDIX A. STRAIN EQUIVALENCE AND CG

The purpose of this section is to show the identity (29)

$$\overline{\varepsilon} : \left\langle \mathbb{C} : \varepsilon^{k+1} \right\rangle_Q = \left\langle \varepsilon^k : \mathbb{C} : \varepsilon^{k+1} \right\rangle_Q, \tag{A1}$$

for linear CG. For this purpose, we need some terminology and background for the linear conjugate gradient method, which is standard[80(section 5.1)]. Let us consider a Hilbert space V with inner product $(\cdot, \cdot)_V$, together with a bounded, self-adjoint and positive semi-definite linear operator $A \in L(V)$, and a given right-hand side b. We wish to solve the linear equation

$$Ax = b, \tag{A2}$$

for $x \in V$, which we rephrase as the critical point equation associated to the quadratic function

$$\phi : V \to \mathbb{R}, \quad \phi(x) = \frac{1}{2} (x, Ax)_V - (b, x)_V. \tag{A3}$$

A sequence of directions $d_0, d_1, \ldots$ is called A-conjugate provided $d_i \neq 0$ for all i and the condition

$$(Ad_i, d_j) = 0, \tag{A4}$$

holds for all $i \neq j$. A-conjugacy (A4) may be thought of as a generalized orthogonality condition between vectors. For any starting point $x^0 \in V$ and a sequence of A-conjugate directions, the conjugate directions method seeks iterates in the form

$$x^{k+1} = x^k + \alpha_k d^k \tag{A5}$$

with α_k determined through a line search

$$\alpha_k = \arg \min_\alpha \phi(x^k + \alpha \, d^k). \tag{A6}$$

It is not difficult to see that the identity

$$\alpha_k = -\frac{(g^k, d^k)_V}{(d^k, Ad^k)_V}, \tag{A7}$$

holds in terms of the gradient

$$g^k = Ax^k - b. \tag{A8}$$

Due to the A-conjugacy (A4), it can be shown that, for any $k > 0$, the step sizes α_i $(i \leq k)$ are actually *jointly minimal*, that is, the identity

$$(\alpha_0, \dots, \alpha_k) = \arg \min_{(\tilde{\alpha}_0, \dots, \tilde{\alpha}_k)} \phi\left(x^0 + \sum_{i=0}^k \tilde{\alpha}_i \, d^i\right), \tag{A9}$$

encodes that previous progress is actually preserved by a conjugate direction method. The conjugate gradient method arises by applying Gram–Schmidt orthogonalization to the negative gradient direction, that is,

$$d^k = -g^k + \sum_{i=0}^{k-1} \frac{(g^k, d^i)_V}{\|d^i\|_V^2} \, d^i \quad \text{with} \quad \|d^i\|_V^2 \equiv (d^i, d^i)_V. \tag{A10}$$

Through algebraic manipulations, it is straightforward to see that all but the last term vanish, and we are led to the expression

$$d^k = -g^k + \frac{\|g^k\|_V^2}{\|g^{k-1}\|_V^2} \, d^{k-1}, \quad k \geq 1, \tag{A11}$$

and practical implementations of the conjugate gradient method.[25] Of relevance to us is the following immediate consequence of Equations (A7) and (A11): the current gradient is orthogonal to the previous conjugate directions

$$(g^k, d^i)_V = 0, \quad i < k. \tag{A12}$$

To apply this technology to computational homogenization, we set

$$V = L^2(Q; \text{Sym}(d)), \tag{A13}$$

endowed with the inner product

$$(\varepsilon_1, \varepsilon_2)_V = \left\langle \varepsilon_1 : \mathbb{C}^0 : \varepsilon_2 \right\rangle_Q, \tag{A14}$$

for a fixed (possibly anisotropic) reference material $\mathbb{C}^0$. Moreover, for prescribed macroscopic strain $\bar{\varepsilon} \in \text{Sym}(d)$, we set

$$A\varepsilon = \Gamma^0 : \mathbb{C} : \varepsilon \quad \text{and} \quad b = -\Gamma^0 : \mathbb{C} : \bar{\varepsilon}. \tag{A15}$$

Upon solving the linear equation (A2) for the strain fluctuation $\tilde{\varepsilon}$, the solution ε to the balance equation (3) is recovered via $\varepsilon = \bar{\varepsilon} + \tilde{\varepsilon}$, see Zeman et al.[26] If we choose $\tilde{\varepsilon}^0 = 0$, we may write the kth CG iterate in the form

$$\tilde{\varepsilon}^k = \sum_{i=0}^k \alpha_i D^i, \tag{A16}$$

where we write an uppercase D^i instead of d^i for the search direction to emphasize that this is actually a (compatible) strain field. In particular, we observe

$$
\begin{aligned}
\left\langle \varepsilon^k : \mathbb{C} : \varepsilon^{k+1} \right\rangle_Q &= \left\langle \overline{\varepsilon} : \mathbb{C} : \varepsilon^{k+1} \right\rangle_Q + \left\langle \tilde{\varepsilon}^k : \mathbb{C} : \varepsilon^{k+1} \right\rangle_Q \\
&= \overline{\varepsilon} : \left\langle \mathbb{C} : \varepsilon^{k+1} \right\rangle_Q + \left\langle \tilde{\varepsilon}^k : \mathbb{C} : \varepsilon^{k+1} \right\rangle_Q.
\end{aligned}
\tag{A17}
$$

Taking a closer look at the term

$$
\begin{aligned}
\left\langle \tilde{\varepsilon}^k : \mathbb{C} : \varepsilon^{k+1} \right\rangle_Q &= \left\langle \sum_{i=0}^{k} \alpha_i D^i : \mathbb{C} : \varepsilon^{k+1} \right\rangle_Q \\
&= \sum_{i=0}^{k} \alpha_i \left\langle D^i : \mathbb{C} : \varepsilon^{k+1} \right\rangle_Q,
\end{aligned}
\tag{A18}
$$

and using the compatibility of $D^i = \Gamma^0 : \mathbb{C}^0 : D^i$,[55] we observe

$$
\begin{aligned}
\left\langle \tilde{\varepsilon}^k : \mathbb{C} : \varepsilon^{k+1} \right\rangle_Q &= \sum_{i=0}^{k} \alpha_i \left\langle D^i : \mathbb{C} : \varepsilon^{k+1} \right\rangle_Q \\
&= \sum_{i=0}^{k} \alpha_i \left\langle \Gamma^0 : \mathbb{C}^0 : D^i : \mathbb{C} : \varepsilon^{k+1} \right\rangle_Q \\
&= \sum_{i=0}^{k} \alpha_i \left(\Gamma^0 : \mathbb{C}^0 : D^i, (\mathbb{C}^0)^{-1} : \mathbb{C} : \varepsilon^{k+1} \right)_V \\
&= \sum_{i=0}^{k} \alpha_i \left(D^i, \Gamma^0 : \mathbb{C}^0 : (\mathbb{C}^0)^{-1} : \mathbb{C} : \varepsilon^{k+1} \right)_V \\
&= \sum_{i=0}^{k} \alpha_i \left(D^i, \Gamma^0 : \mathbb{C} : \varepsilon^{k+1} \right)_V \\
&= \sum_{i=0}^{k} \alpha_i \left(D^i, \Gamma^0 : \mathbb{C} : (\overline{\varepsilon} + \tilde{\varepsilon}^{k+1}) \right)_V \\
&= \sum_{i=0}^{k} \alpha_i \left(D^i, G^{k+1} \right)_V \\
&= 0,
\end{aligned}
\tag{A19}
$$

where we used that the operator $\Gamma^0 : \mathbb{C}^0$ is self-adjoint w.r.t. the inner product (A14) and that the orthogonality condition (A12) holds between the search directions D^i and the gradient G^{k+1} for $i \leq k$. Thus, Equation (A1) is a direct consequence of the previous ideas and Equation (A17).

As a side remark, if $\tilde{\varepsilon}^0 \neq 0$ is chosen as the initial guess, we still get the identity

$$
\left\langle \overline{\varepsilon} : \mathbb{C} : \varepsilon^{k+1} \right\rangle_Q = \left\langle \left(\overline{\varepsilon} + \sum_{i=0}^{k} \delta_i D^i \right) : \mathbb{C} : \varepsilon^{k+1} \right\rangle_Q,
\tag{A20}
$$

for any coefficients δ_i. In particular, invoking the estimate (14) for $\varepsilon = \varepsilon^{k+1}, \overline{\xi} = \overline{\varepsilon}$ and

$$
\xi = \overline{\varepsilon} + \sum_{i=0}^{k} \delta_i D^i,
\tag{A21}
$$

gives

$$\left| \overline{\varepsilon} : \left\langle \mathbb{C} : \varepsilon^{k+1} \right\rangle_Q - \overline{\varepsilon} : \mathbb{C}^{\text{eff}} : \overline{\varepsilon} \right| \leq L \, \|\varepsilon^{k+1} - \varepsilon^*\|_{L^2} \left\| \overline{\varepsilon} + \sum_{i=0}^{k} \delta_i \, D^i - \varepsilon^* \right\|_{L^2}. \tag{A22}$$

As we may choose the coefficients δ_i to our liking, we even obtain

$$\left| \overline{\varepsilon} : \left\langle \mathbb{C} : \varepsilon^{k+1} \right\rangle_Q - \overline{\varepsilon} : \mathbb{C}^{\text{eff}} : \overline{\varepsilon} \right| \leq \min_{(\delta_0, \ldots, \delta_k)} L \, \|\varepsilon^{k+1} - \varepsilon^*\|_{L^2} \left\| \overline{\varepsilon} + \sum_{i=0}^{k} \delta_i \, D^i - \varepsilon^* \right\|_{L^2}. \tag{A23}$$

Thus, we also expect a superaccuracy result for the computed stress on the generated Krylov subspaces, however, in a slightly more complicated form.